J. Fluid Mech. (1988), *vol.* 189, *pp.* 571–598
Printed in Great Britain

Differential mixing in a stratified fluid

By T. MAXWORTHY† AND S. G. MONISMITH‡
Centre for Water Research, University of Western Australia,
Nedlands, WA 6009, Australia

(Received 5 June 1986 and in revised form 20 June 1987)

We present an experimental and theoretical study of the effects of localized mixing on a stratified fluid contained in a reservoir. In the experiments, mixing is accomplished by means of a vertically oscillating, horizontal grid located near the water surface at one end of the reservoir. Once the grid is set in motion, a mixed layer forms immediately beneath it. As this layer deepens, a horizontal pressure gradient builds up which drives an outflow of mixed fluid into the unmixed interior of the reservoir. This outflow slows, and eventually brings to a halt, mixed-layer deepening under the grid. At this equilibrium depth, the vertical velocity of the entrainment interface induced by the outflow exactly equals the velocity at which the entrainment interface would move downwards because of mixing. This equilibrium state persists until the outflow intrusion is blocked by the far wall of the reservoir, at which time deepening resumes under the grid. Asymptotically, the fluid reaches a state in which mixed-layer deepening is independent of position.

1. Introduction

In virtually all naturally occurring fluid mixing processes, the spatial distribution of the mixing action is non-uniform. However, previous studies of such processes have consistently used a local, vertical, one-dimensional approximation with no lateral communication between adjacent regions. Although this approach is a useful first step, as our needs become more specific, more complex physical processes must be included in predictive numerical models.

To demonstrate the higher order of complexity inherent in spatially varying mixing, we start by considering two typical cases of general interest. In the first, a barotropic tidal flow exists adjacent and parallel to a coastline. Models of this flow advanced by Simpson & Hunter (1974) or Maxworthy (1984) predict that a front will form at that distance off the coast where tidal, turbulent kinetic energy can just completely mix the surface heat input and/or any pre-existing stratification. Hopfinger & Linden (1982) have studied this problem in the context of a one-dimensional budget of turbulent kinetic energy. The question however arises: what happens to this mixed fluid? Clearly, it must collapse into the adjacent, less well-mixed and hence stratified fluid, flowing as an intrusion at its level of neutral buoyancy. What effect does this flow have on the mixing process itself, and hence on the location of the front?

A related, and environmentally important case is that of differential wind mixing

† Permanent address: Departments of Mechanical and Aerospace Engineering, University of Southern California, Los Angeles, CA 90089-1453, USA.

‡ Present address: Environmental Fluid Mechanics Laboratory, Department of Civil Engineering, Stanford University, Stanford, CA 94305-4020, USA.

in a stratified lake or reservoir. As observed in several field studies on the Wellington Reservoir in Western Australia (see Imberger & Parker 1985), patchiness in the wind stress field due to the sheltering effects of surrounding hills leads to substantial horizontal variations in mixed-layer depth and temperature. The horizontal transport associated with collapse of these horizontal density gradients can dominate the exchange of fluid between the reservoir's side arms and its main basin (Imberger 1982). In this case, since the winds are inherently unsteady, it is important to know the timescales of the collapse as well as the ways in which mixed-layer deepening is modified by spatial variations in forcing.

Two other mixing processes which result in similar effects are boundary mixing, which has been examined by Ivey & Corcos (1982), and lake destratification by bubble plumes, studied by Kranenburg (1979). In both of these experimental studies, localized mixing led to global changes in the density field, and eventually to the homogenization of the fluid.

The processes described in the preceding examples can be reduced to somewhat simpler and more general terms. When a stratified fluid is mixed locally, horizontal density gradients and, hence, horizontal pressure gradients are created that drive a flow of mixed fluid away from the mixing region. Several experiments have investigated the flow resulting from a single mixing event, i.e. the situation where mixing occurs on a timescale much shorter than the time required for the fluid to respond (Wu 1969; Amen & Maxworthy 1980). When the mixing only lasts a short time, the volume of mixed fluid is fixed so that as the mixed region grows in horizontal extent, it contracts vertically.

However, when mixing is maintained, the outflow persists for as long as the fluid in the mixing region is at a density different from that of the surrounding fluid. If the fluid were effectively infinite in horizontal extent, the mixing process could go on indefinitely with unmixed fluid being continually drawn into the mixing region. In contrast, if the fluid is bounded horizontally, the entire body of fluid must eventually become mixed. Thus, the tidal flow mentioned above would typify the case of a semi-infinite fluid, while the reservoir flow would typify that of a bounded fluid.

In §2 of this paper we shall present a model of the mixing process that combines a simple model of an outflow intrusion with a simple model of one-dimensional deepening, one pertinent to the experimental study of differential deepening driven by an oscillating grid as presented in §§3–5. Although the model is based on the particular properties of grid-generated turbulence, the results can be generalized to include other types of turbulent mixing.

2. Theory

2.1. *Introduction*

The response of a confined stratified fluid to localized mixing can be broken down into two main aspects: the process of turbulent entrainment across a density interface; and the circulation response, i.e. the flow of fluid from the mixing region into the unmixed ambient fluid, plus any mean circulation in the body of the reservoir driven by the outflow. These processes have been considered separately in previous studies; in this section, we shall develop a theory of the fluid response also based on such an isolation of the processes. We shall assume that entrainment in the mixing region is always a vertical, one-dimensional process. One implication of this assumption is that we neglect any possible contribution to mixed-layer deepening made by shear across the interface due to the outflow from the mixed region. We also

assume that the outflow behaviour is determined solely by the vertical extent of the mixed region, and by the pressure gradient associated with horizontal density differences due to localized mixing; any effects of the decaying turbulence exported from the mixed region will be neglected.

Reviews of one-dimensional deepening of mixed layers in stratified fluids can be found in a number of references (e.g. Turner 1973; Sherman, Imberger & Corcos 1978). For the purposes of this study, any of the several available models of the entrainment process can be used. The circulation response is somewhat more complicated than the entrainment process, however. Although the dynamics of viscous and inertial intrusions formed by inflows into linearly stratified ambients (Maxworthy 1972; Manins 1976; Imberger, Thompson & Fandry 1976) and of various types of two-layered gravity currents (Simpson 1982) are well understood, descriptions of the behaviour of these intrusive flows are usually most applicable to a flow at some distance from its source. The present case requires prediction of the flow rate based on the pressure gradient which develops due to differential mixing. In the absence of detailed theories pertinent to the flows observed in our experiments, we shall use scaling analysis to obtain two estimates of the dependence of the rate of outflow from the mixed region on the experimental parameters. This information about the outflow will then be used to describe the effect of spatial variability in the mixing rate on mixed-layer deepening.

2.2. *Deepening of a grid-stirred layer in a linearly stratified fluid*

2.2.1. *One-dimensional deepening*

The basis of our model of differential deepening is the parameterization of Turner's (1968) (see also Hopfinger & Toly 1976) grid-stirring experiments given in Denton & Wood (1982). For the limiting case of an infinite Péclet number, they find that Turner's entrainment results can be accurately represented by the formula

$$\frac{\mathrm{d}h}{\mathrm{d}t} = 1.18u(h)\,(1+0.41\,Ri^{\frac{3}{2}})^{-1}. \tag{1}$$

Here h is the depth of the mixed layer and $u(h)$ the turbulent velocity scale at the location of the density interface (but measured in the absence of an interface, cf. Hopfinger & Toly 1976). The local Richardson number Ri is defined as

$$Ri = g' l_{\mathrm{t}}(h)\, u^{-2}, \tag{2}$$

where g' is the interfacial buoyancy jump, and $l_{\mathrm{t}}(h)$ the turbulent lengthscale at the location of the interface. The turbulent length and velocity scales are evaluated using the experimental data of Hopfinger & Toly (1976):

$$l_{\mathrm{t}} = C_1 h \tag{3}$$

and

$$u = C_2 K h^{-1}. \tag{4}$$

In terms of the amplitude of oscillation of the grid (stroke) S, frequency f, and mesh spacing M,

$$K = S^{\frac{3}{2}} M^{\frac{1}{2}} f. \tag{5}$$

The constants C_1 and C_2 depend on the grid's solidity, the shape of the bars, S, M and f; they have typically values (for $S = 4$ cm, $M = 5$ cm and $f = 3$ Hz) of 0.26 and 0.29 respectively (Hopfinger & Linden 1982). The parameter K is known as the 'grid action' (e.g. Long 1978).

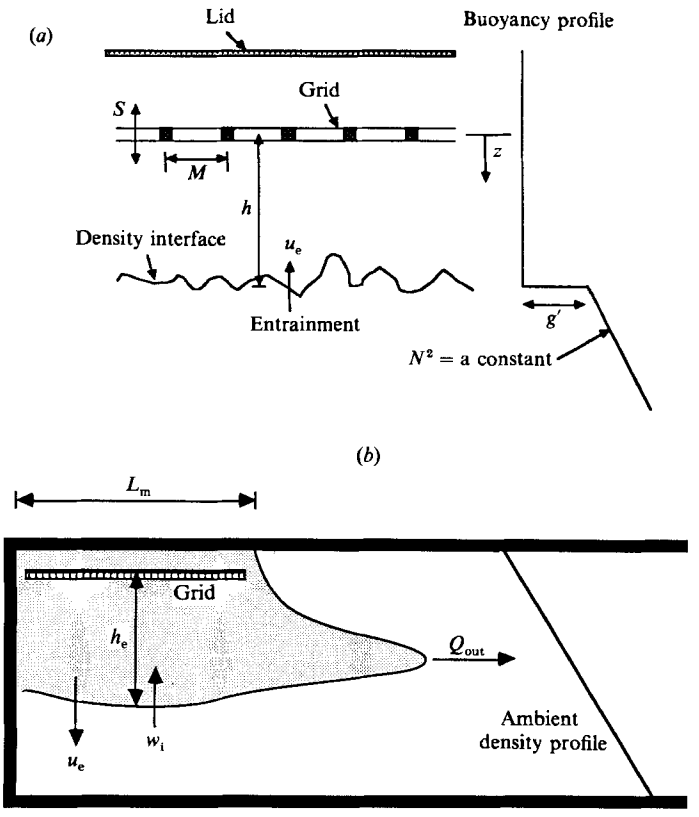

FIGURE 1. Definition sketch for (*a*) one-dimensional mixed-layer deepening in a linearly stratified fluid; (*b*) localized mixed-layer deepening in a semi-infinite linearly stratified fluid.

To find $h(t)$ in the absence of outflow effects, the density profile must be specified. If the density initially varies linearly with height, and the geometry is as is sketched in figure 1 (*a*),

$$g' = \tfrac{1}{2}N^2 h, \tag{6}$$

so that (1) becomes

$$\frac{\mathrm{d}h}{\mathrm{d}t} = (1.18C_2 K h^{-1})(1+C_3 h^6 y^{-6})^{-1}, \tag{7}$$

where the scale length y† is defined by

$$y = K^{\frac{1}{3}}N^{-\frac{1}{2}}, \tag{8}$$

and $C_3 = 0.15C_1^{\frac{3}{2}}C_2^{-3} = 0.82$. Equation (7) can be recast in terms of the dimensionless variables $\eta = (hy^{-1})$ and $\tau = Nt$, yielding

$$\frac{\mathrm{d}\eta}{\mathrm{d}\tau} = 0.34(\eta + 0.82\eta^7)^{-1}, \tag{9}$$

which when integrated, assuming that $\eta(0) = 0$, yields

$$\eta^2 + 0.21\eta^8 = 0.68\tau. \tag{10}$$

† y is the distance over which turbulent diffusion with eddy diffusivity K would diffuse any property in one buoyancy period (i.e. in a time interval of length N^{-1}).

Hence two asymptotic laws arise:

$$\eta \approx 0.8\tau^{\frac{1}{2}}, \quad \tau \leqslant 1, \tag{11}$$

and

$$\eta \approx 1.15\tau^{\frac{1}{8}}, \quad \tau \gg 1. \tag{12}$$

The short-time asymptotic law describes the deepening that takes place before the stratification can affect the deepening process (Turner 1973). The exponent in (12), the long-time deepening law, is determined mainly by the decay law, (4), and by the $Ri^{-\frac{3}{2}}$ term in (1); it differs only slightly from the exponents given by Long (1978) ($\frac{1}{9}$) and Linden (1975) ($\frac{2}{15}$). The transition from the rate given by (11) to the much slower rate given by (10) occurs at $\eta \approx 1.3$.

Equations (11) and (12) are based on the simplifying assumption that the virtual origin (Hopfinger & Toly 1976) of the turbulence decay law coincides with the plane of the grid, and that the plane of the grid is much closer to the upper surface than it is to the entrainment interface. These assumptions should have little effect on the accuracy of the long-term deepening law (12). The short-term law (11) is correct provided that h is defined as the distance from the virtual origin (approximately 1 cm behind the grid). More accurate predictions of the transition could be obtained by including both effects, but this would complicate the algebra and add little of value.

2.2.2. *Differential deepening in a semi-infinite fluid*

Next, suppose that the grid is of some finite length L_m, and sits at one end of a fluid of semi-infinite horizontal extent (figure 1*b*). As before, the grid is set in motion at $t = 0$. Experiments on mixed-layer collapse and intrusions (for example, Wu 1969) have shown that the initial collapse of a mixed region into a stratified fluid takes place in a time T_c, approximately equal to one buoyancy period, i.e.

$$T_c = 2\pi N^{-1}. \tag{13}$$

For times much shorter than T_c, deepening will be one-dimensional because the buoyancy forces involved in the collapse process itself require a time of T_c to set the fluid in motion. Thus, the mixed-layer depth will initially satisfy (11) (with the same provisos as above).

As the layer deepens, a pressure difference $P \sim \rho N^2 h^2$ will develop, eventually forcing mixed fluid out of the mixing region at its level of neutral buoyancy. If we assume that an inertia–buoyancy balance must prevail at the edge of the mixing region, the volume flux out of the mixed layer, Q_{out}, will be of the form (Manins 1976)

$$Q_{out} \sim Nh^2. \tag{14}$$

This parameterization of Q_{out} will only be valid if turbulent shear stresses are much smaller than inertial forces; this requires

$$h^2 \gg \nu_t T_{out} \tag{15}$$

where ν_t is an appropriate 'eddy' viscosity, and T_{out} is the timescale characterizing establishment of the outflow (e.g. Batchelor 1967). Since the pressure imbalance initially existing across the vertical boundary between the mixing region and the rest of the fluid must be transmitted to the rest of the mixing region by the propagation of internal waves, the appropriate timescale is the wave timescale,

$$T_{out} \sim L_m(Nh)^{-1}. \tag{16}$$

For grid-generated turbulence, $\nu_t \sim K$; this means that, from (15) and (16),

$$R = h^3(L_m y^2)^{-1} \gg 1 \tag{17}$$

for an inertia-buoyancy balance to be possible. However, in the experiments, $R \sim 1$; hence, an inertia-buoyancy balance may not be possible.

Rather than assume an inertia-buoyancy balance, an alternative model balances the pressure gradient associated with the horizontal density gradient against the turbulent shear stress arising from the mean flow in the mixing region that supplies the outflow intrusion. The basic premise of this analysis is that fluid enters the mixing region via the entrainment interface and leaves the mixing region via the outflow intrusion. The viscous–buoyancy balance is

$$\nu_t \partial^2_{zz} u \sim \rho^{-1} \partial_x p,$$

which we estimate as

$$KUh^{-2} \sim N^2 h^2 L_m^{-1},$$

where U is the velocity scale of the horizontal flow in the mixing region. Here we have used L_m as the appropriate horizontal lengthscale because it is the horizontal lengthscale of the flow.†

Using this viscous–buoyancy model, we obtain a second estimate for Q_{out} (say Q'_{out}),

$$Q'_{out} \sim N^2 h^5 K^{-1} L_m^{-1} \sim N h^2 R \sim R Q_{out}. \tag{18}$$

One interpretation of (18) is that when $R \gg 1$, a viscous–buoyancy balance permits a larger flow than an inertia–buoyancy balance does. In this case, the flow rate would be set by inertial effects; i.e. an hydraulic control (as in Armi 1986) at the edge of the mixing region would determine the outflow rate. However, when $R \ll 1$, the outflow rate is controlled by friction in the mixing region. In either case, outside the mixing region, ν_t drops rapidly as the turbulence decays (in our experiments, the intrusions appeared to be laminar). The outflow intrusions themselves may therefore exhibit an inertia–buoyancy balance appropriate to the supply of mixed fluid which is controlled by either viscous or inertial effects depending on the value of R.

In any event, the outflow will induce a *vertical velocity* w_i at the entrainment interface as indicated in figure 1(*b*). If $w_i < u_e$, then the entrainment interface will propagate downwards at a net speed equal to $(u_e - w_i)$. If $w_i = u_e$, the entrainment interface will remain fixed in space and the layer will not deepen. Thus, in contrast to the one-dimensional case, the entrainment velocity u_e will no longer be equal to the rate of mixed-layer deepening, dh/dt. Both the entrainment rate and outflow rate depend on the mixed-layer depth, entrainment decreasing with increasing depth and outflow increasing; thus, as the layer deepens, the net rate of deepening, $(u_e - w_i)$, will decrease; eventually, at some equilibrium depth, the layer will stop deepening.

Using (1) to compute u_e, assuming that the equilibrium depth is sufficiently large that we can neglect the constant term appearing in the denominator of (1), and using (14) or (18) to compute the induced flow, we can estimate the non-dimensional equilibrium depth, η_e:

If inertial forces are important,

$$\eta_e \sim (L_m/y)^{\frac{1}{5}}. \tag{19}$$

† This is shown by noting that the vertical flow that supplies the outflow should be approximately uniform along the length of the mixing interface. Therefore, by continuity, the net flow towards the outflow boundary (i.e. to the right in figure 1*b*) must increase linearly with increasing distance from the wall at the left of figure 1(*b*). Given a constant eddy viscosity (at least independent of ζ – see figure 3), the pressure gradient must be approximately linear in ζ, so that the lengthscale over which it varies must be L_m.

If turbulent shear stresses control the flow,

$$\eta_e \sim (L_m/y)^{\frac{1}{6}}. \tag{20}$$

In both cases, the equilibrium depth is only weakly dependent on the aspect ratio (L_m/y).

The flows in our experiments, like many natural flows (see §6), fall into the class of flows for which $R \sim 1$. In this case, either (or neither) scaling may be correct, and so we must appeal to the experimental results to choose between the two possibilities.

2.2.3. *Differential deepening of a confined fluid*

If the intrusion is in inertia–buoyancy balance, the front of the outflow from the mixing region will travel at a speed of approximately Nh_e (Manins 1976). If the fluid were truly infinite the situation sketched in figure 1(*b*) could persist indefinitely. However, if the fluid is bounded the outflow will eventually reach the far wall; and, before it does, all of the internal shear wave with vertical wavelengths greater than h_e, generated by initiation of the outflow, will have reached the far wall, reflected off that wall and be travelling back towards the mixing region (Manins 1976). Furthermore, the intrusion will be propagating into a region in which the density field has already been modified by those shear waves; consequently, it experiences progressively more drag (Foster & Saffman 1970) while at the same time, the driving force is simultaneously reduced as the shear waves reduce the density gradient ahead of the intrusion. Thus, on a timescale of order (L/Nh_e), where L is the distance from the edge of the mixing region to the far wall, the intrusion will become blocked by the rear wall, the driving pressure gradient will weaken, and Q_{out} will decrease. The mixed layer will resume deepening, because $u_e(h)$, which is not affected by the outflow, will then be larger than w_i.

The experimental results suggest that once blocking has taken place, the mixed layer eventually deepens in a quasi-one-dimensional fashion, i.e. the layer deepens at the same rate near the grid as in the body of the fluid. This is because blocking weakens the density gradient in the fluid between the intrusion and the far wall; in effect, the intrusion forces open the isopycnals bounding it (Foster & Saffman 1970). Thus, the density profile ahead of the intrusion becomes more and more like the density profile behind the head of the intrusion. If that is the case, the rate at which fluid is entrained across the interface region is equal to the total gain in volume of the mixed layer (which then also includes the blocked region). In other words,

$$u_e L_m = \frac{dh}{dt} L_t, \tag{21}$$

giving

$$\frac{dh}{dt} = u_e \frac{L_m}{L_t}. \tag{22}$$

The net rate of entrainment, dh/dt, is simply the local rate of entrainment multiplied by the ratio of the length of the region where mixing is taking place to the total length of the reservoir. Using (9), (22) can be integrated to give, for $\tau \gg 1$,

$$\eta \sim 1.2 \left(\frac{L_m}{L_t}\right)^{\frac{1}{8}} \tau^{\frac{1}{8}}. \tag{23}$$

Thus, η (or h) has exactly the same time dependence for the two-dimensional mixing process we are modelling as it has for the one-dimensional process. Additionally,

the dependence of $h(t)$ on (L_m/L_t) is weak; for the experiments, this factor is $(125/550)^{\frac{1}{8}} = 0.83$.

2.3. *Deepening by grid-stirring in a two-layered fluid*

The case of mixed-layer deepening by grid stirring in a two-layered fluid is very similar to that discussed above. Consider first the one-dimensional deepening rate. As in the linear case, a lengthscale, say x, can be defined as

$$x = KB_0^{-\frac{1}{2}}, \tag{24}$$

where the mixed-layer buoyancy,

$$B_0 = g_0' h_0 = g'(t)\, h(t), \tag{25}$$

is constant, and the mixed-layer depth h is as shown in figure 2. The natural timescale of deepening is

$$T_d = x^2 K^{-1} = KB_0^{-1}. \tag{26}$$

Thus using (1)–(5), and the dimensionless variables

$$\tau = tT_d^{-1} \tag{27a}$$

and

$$\eta = hh_0^{-1}, \tag{27b}$$

the entrainment law becomes (using the same assumptions made in §2.2.1):

$$\frac{d\eta}{d\tau} = \frac{0.34(x/h_0)^2}{\eta + 2.22(h_0/x)^3 \eta^4}. \tag{28}$$

Equation (28) can be integrated to give

$$0.5\eta^2 + 0.44\left(\frac{h_0}{x}\right)^3 \eta^5 = 0.34\left(\frac{x}{h_0}\right)^2 \tau + \phi, \tag{29}$$

where ϕ is an integration constant. Because the second term on the left-hand side of (29) is exactly zero until $\eta = 1$, i.e. until the turbulent front actually reaches the interface, two deepening laws are observed. When $\eta < 1$,

$$\eta = 0.7\frac{x}{h_0}\tau^{\frac{1}{2}}. \tag{30}$$

whereas, when $\eta > 1 (h > h_0)$, (29) is satisfied. The integration constant can be determined by matching the two solutions at $\eta = 1$, viz.

$$\phi = 0.44\left(\frac{h_0}{x}\right)^3. \tag{31}$$

When $\eta \gg 1$, the asymptotic deepening law is

$$\eta \approx 0.95\frac{x}{h_0}\tau^{\frac{1}{5}}. \tag{32}$$

The effects of horizontal variations in mixing should be similar to those described above for linear stratifications. However, because there are now two important parameters, (x/h_0) and (x/L_m), the scaling is more complex and less amenable to experimental verification. Consequently, we shall not attempt to analyse the equilibration process for this case. However, the long-term, quasi-one-dimensional

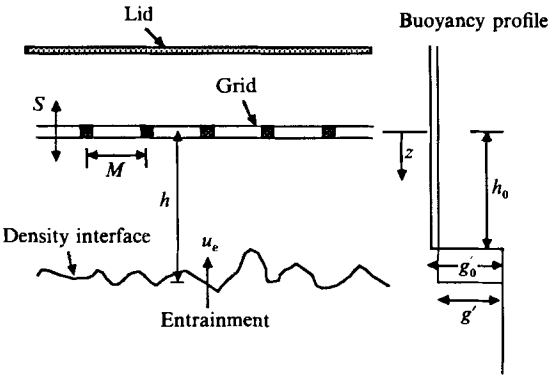

FIGURE 2. Definition sketch for one-dimensional mixed-layer deepening in a two-layer fluid.

entrainment law, valid once rear-wall blocking of the outflow has taken place, can be calculated using the one-dimensional asymptotic deepening law to be

$$\eta \approx 0.95 \frac{x}{h_0} \frac{L_m}{L^{\frac{1}{5}}} \tau^{\frac{1}{5}}. \tag{33}$$

As in the case of linear stratification, because the deepening rate decreases as the mixed-layer depth increases, the dependence of the net deepening rate on the ratio of mixed to unmixed areas is weak.

3. Experimental apparatus and procedure

The experimental apparatus is shown in figure 3. All the experiments described were run in a flume 5.5 m long by 0.5 m wide and 0.6 m deep. At one end of the flume we placed a Perspex stirring grid 1.5 m long with 1 cm square bars on 5 cm centres (identical in construction to that used by Turner 1968, and others), which spanned the width of the flume. The grid was driven by a speed-controlled d.c. motor, through a gear reducer and crank-connecting-rod mechanism, at frequencies between 1 and 5 Hz, and at strokes between 1 and 5 cm.

Several inserts were placed in the top of the flume to control the upper boundary of the working fluid. The insert containing the grid itself was used in all of the experiments, whereas other inserts were removed for various experiments. As shown in figure 3, a variable mesh screen was placed at the edge of the mixing region to prevent the formation of a large eddy that otherwise tended to develop at the boundary between the mixed and unmixed fluid, and to provide a more gradual transition between the region of mixing and the rest of the tank. This screen reduced the effective length of the mixing region by approximately 25 cm.

In the first set of experiments the tank was linearly stratified, using salt as the stratifying agent. In the second set of experiments the tank was stratified into two layers. Several four-electrode conductivity probes (described in Stillinger, Helland & Van Atta 1983) mounted on stepper-motor-driven profiles were used to monitor the evolution of the density field. A microcomputer controlled the traversing of the probes and the sampling and storage of their outputs.

Just before the start of each experiment, a dye injector attached to the grid was used to inject dye into the mixing region. As functions of time, the position of the

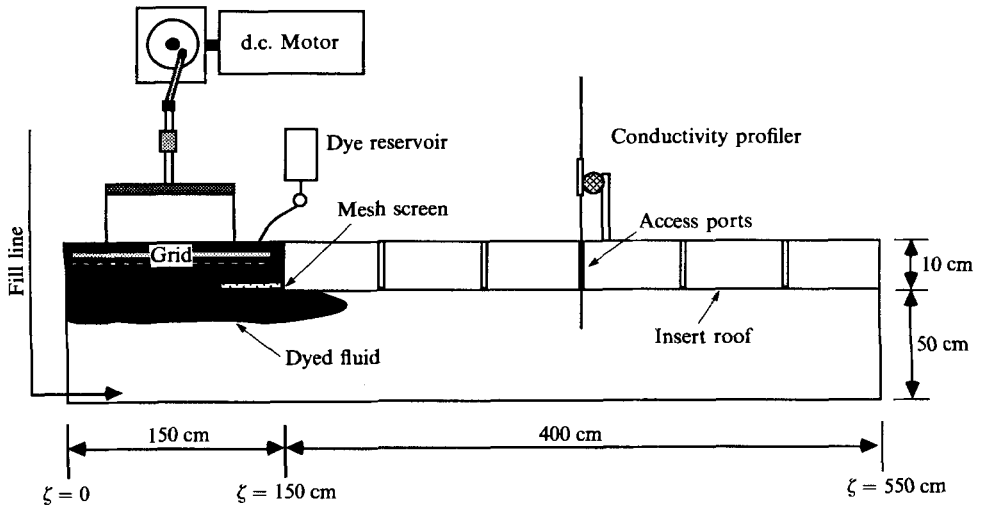

FIGURE 3. Sketch of experimental set-up.

turbulent interface and the length and thickness of the outflow intrusion resulting from the flow of mixed fluid into the interior of the reservoir were then monitored visually and photographically.

The experiments were started with the fluid at rest and lasted between 2 and 6 hours, sufficient time to allow adequate definition of the long-term behaviour of the mixed layer.

4. Experimental results: mixing in a linearly stratified fluid

4.1. *Description of the flow*

In figure 4 we show a sequence of photos of a typical experimental run (Exp 234). The first photo was taken just as the grid was set in motion. We see that the initial motion of the entrainment interface was not accompanied by any outflow from the mixing region. An obvious outflow can be seen in figure 4(*d*), which was taken at $t \approx 2\pi N^{-1}$. By this time, the small-Ri deepening phase was complete and a constant-depth phase was about to begin. Although this is not obvious from the photographic sequence (figure 4), the plot of interface depth h versus time t given in figure 5(*a*) shows the effect very well. The near coincidence of the start of this phase with the start of the outflow was consistent in the majority of our experiments, although the existence of a period of nearly constant mixed-layer depth was not always observed unambiguously.

The interaction of reflected shear-wave modes with the intrusion can be seen in figure 5(*b*), which plots the length of the intrusion as a function of time. The reduction of the head speed seen at approximately $t = 150$ s is typical of our experimental runs; it can be attributed to the passage of the first-mode shear wave (phase speed, $c_1 = NH/\pi$) through the front of the intrusion. Such a wave would have been generated when the outflow started (Manins 1976), and would have travelled to the far wall and back, encountering the intrusion on its return trip at approximately $t = 170$ s. This wave would then reach the edge of the mixing region at $t = 210$ s and communicate to the mixing region the presence of the far wall. As can be seen in figure 5(*a*), the mixed layer began to deepen again at approximately $t = 210$ s. A

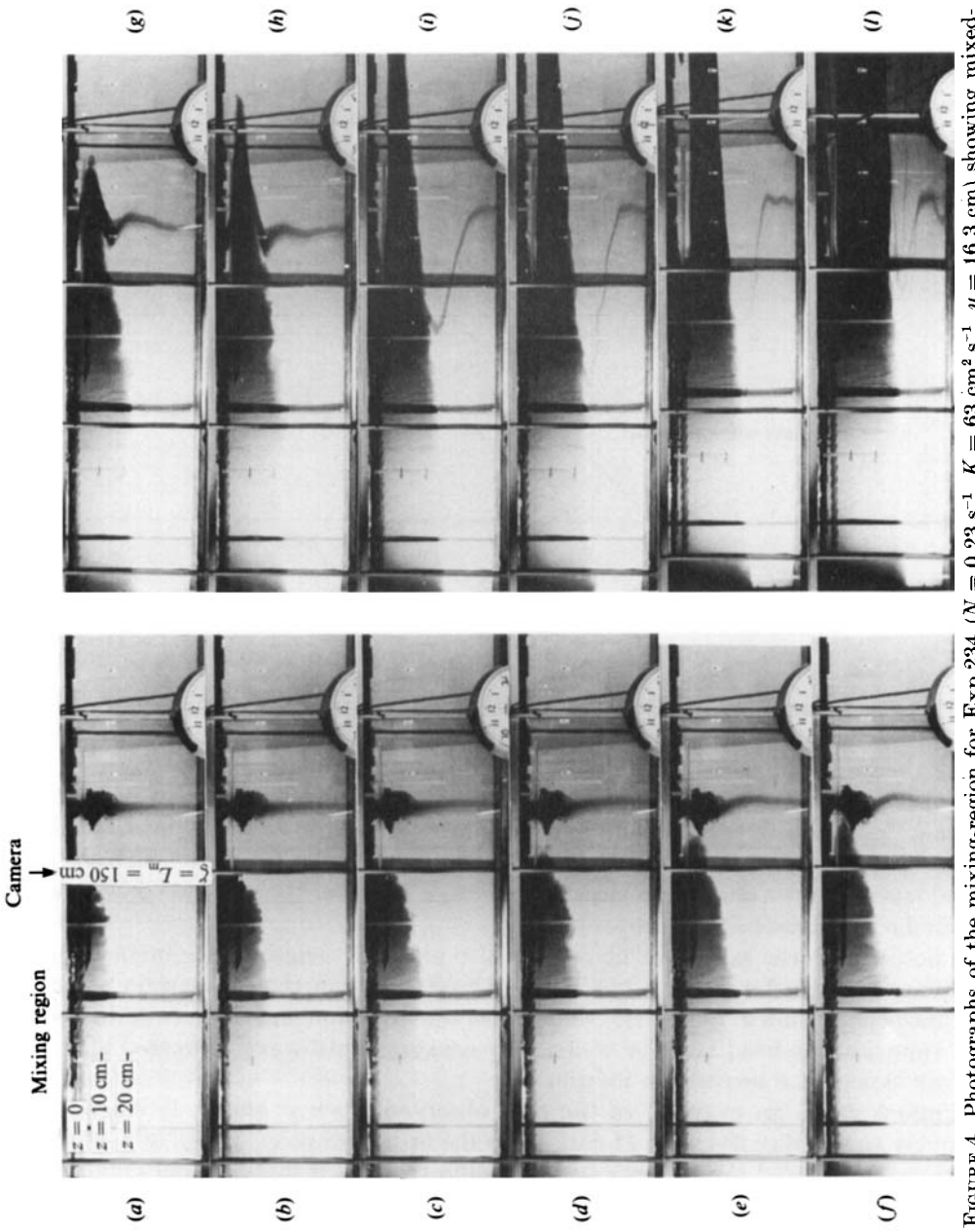

FIGURE 4. Photographs of the mixing-region for Exp 234 ($N = 0.23\ \mathrm{s}^{-1}$, $K = 63\ \mathrm{cm}^2\ \mathrm{s}^{-1}$, $y = 16.3$ cm) showing mixed-layer deepening and intrusion formation. These photos were taken (*a*) 5 s, (*b*) 10 s, (*c*) 23 s, (*d*) 37 s, (*e*) 58 s, (*f*) 74 s, (*g*) 129 s, (*h*) 177 s, (*i*) 365 s, (*j*) 468 s, (*k*) 660 s and (*l*) 2071 s after the grid was set in motion.

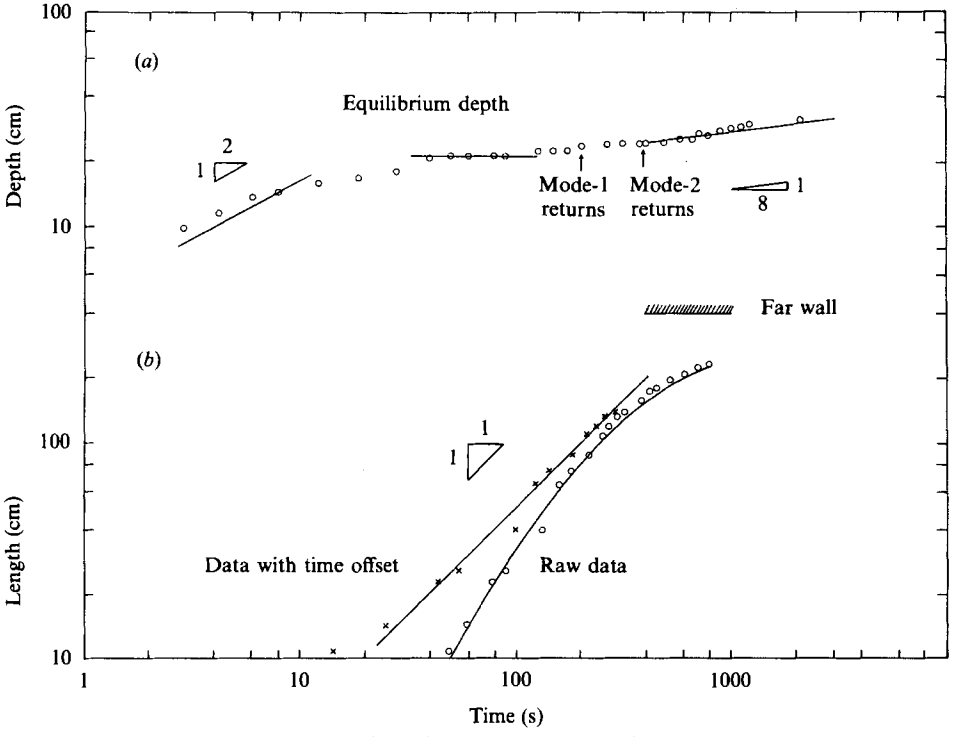

FIGURE 5. (*a*) Mixed-layer depth and (*b*) intrusion length plotted as a function of time for Exp 234.

similar calculation gives a time of 390 s for the return of the second-mode shear wave. Careful examination of the mixed-layer-depth-*vs.*-time curve reveals that before $t = 390$ s, the mixed layer appears to re-equilibrate at a depth of 24 cm between the arrival of the first- and second-mode waves. After $t = 390$ s, the mixed-layer depth appears to increase monotonically while the intrusion begins to slow down, blocked by the back wall. As discussed in §2, once the intrusion has become blocked, the mixed layer resumes deepening at a rate about 17% slower than would be calculated for similar one-dimensional deepening.

In addition to the raw data, figure 5(*b*) also plots the length of the intrusion as a function of time after outflow has begun. Once a shift in the time origin of about 25 s has been included, figure 5(*b*) shows that the intrusion length increased linearly with time, i.e. the head velocity was nearly constant until waves reflected form the far wall slowed the intrusion's motion.

Figure 6 shows an example of the flow observed when y, the scale length, was relatively small (Exp 241; $y = 11$ cm). Both the upstream propagation of a sequence of internal wave and the velocity profile within the slug ($t = 608$ s, 626 s and 671 s) can be seen. An important aspect of the velocity profiles, visible in both figure 6 and figure 4, is the high-velocity flow situated above the outflow and directed towards the mixing region.

A final set of photos, figure 7, shows the development of the flow at a relatively large value of y (Exp 226; $y = 22.6$ cm). Comparing figures 4, 6 and 7, it is clear that the behaviour of the fluid is remarkably similar over the range of values of y obtained in the present experiments.

Figure 8 plots a sequence of density profiles taken 100 cm from the edge of the grid

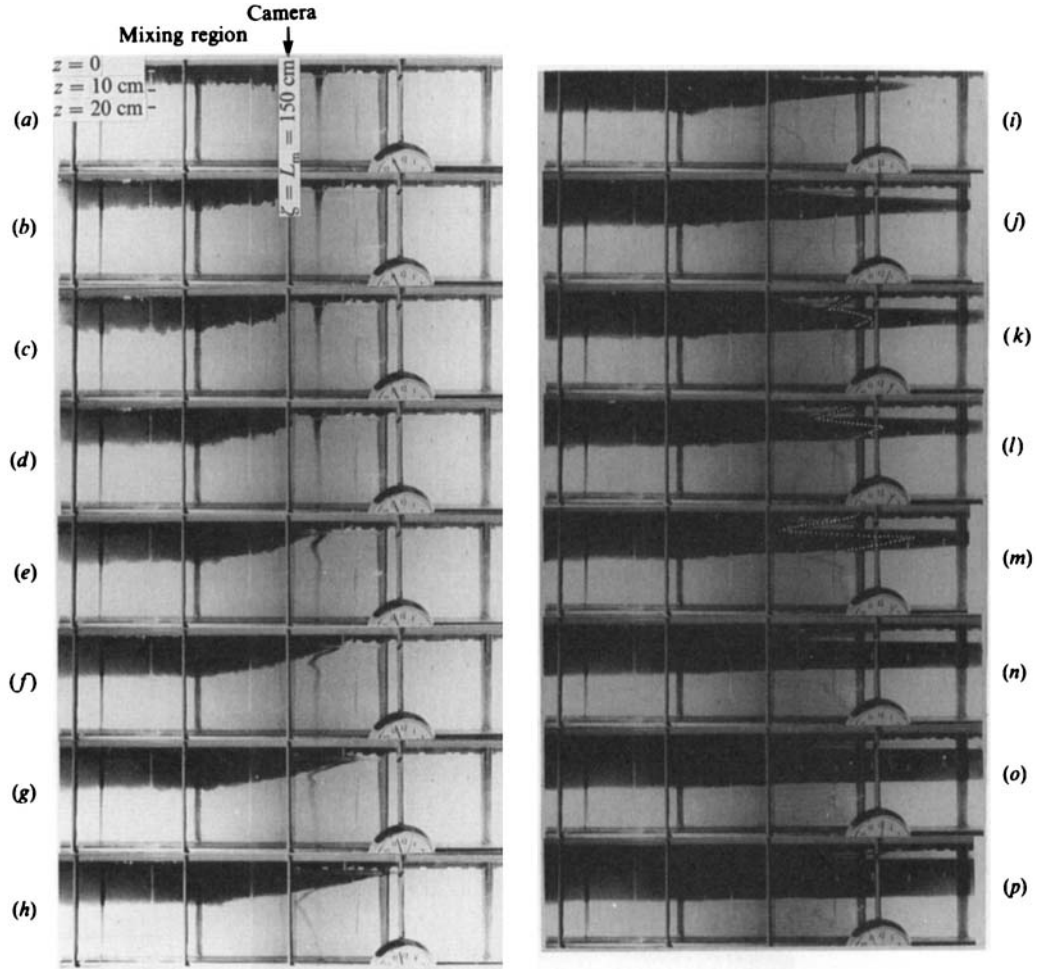

FIGURE 6. Photographs of the mixing region for Exp 241 ($N = 0.38$ s^{-1}, $K = 46.5$ cm^2 s^{-1}, $y = 11.0$ cm) showing mixed-layer deepening and intrusion formation. These photos were taken (*a*) 0 s, (*b*) 5 s, (*c*) 10 s, (*d*) 47 s, (*e*) 57 s, (*f*) 71 s, (*g*) 109 s, (*h*) 148 s, (*i*) 235 s, (*j*) 485 s, (*k*) 608 s, (*l*) 727 s, (*m*) 671 s, (*n*) 1623 s, (*o*) 2986 s and (*p*) 4786 s after the grid was set in motion. The white lines indicate the shape of introduced dye streaks as seen in the original photos from which this figure was made.

throughout the course of Exp 262. These profiles reinforce the description of the flow shown in the photos and in the mixed-layer depth and intrusion-length plots. In particular the second profile ($t = 220$ s) shows that the internal waves generated by the motion of the intrusion reach the probe long before the intrusion does. The effects of blocking can be seen in the distortion of the density field between depths of 6 cm and 18 cm. By the time the third profile was taken ($t = 390$ s), the intrusion had reached the probe as had shear waves reflected off the back wall, although the modification of the profile by intrusions and waves was still quite small. As time passed, a region of weaker density gradient developed, centred first on $z = 20$ cm and then descending to approximately 24 cm, and finally growing to 28 cm in vertical extent by the time the last profile was taken. This region was still stratified after 3400 s, meaning that the outflow was itself stratified. Gradually, recirculation and vertical motions associated with rear-wall blocking acted to homogenize the outflow

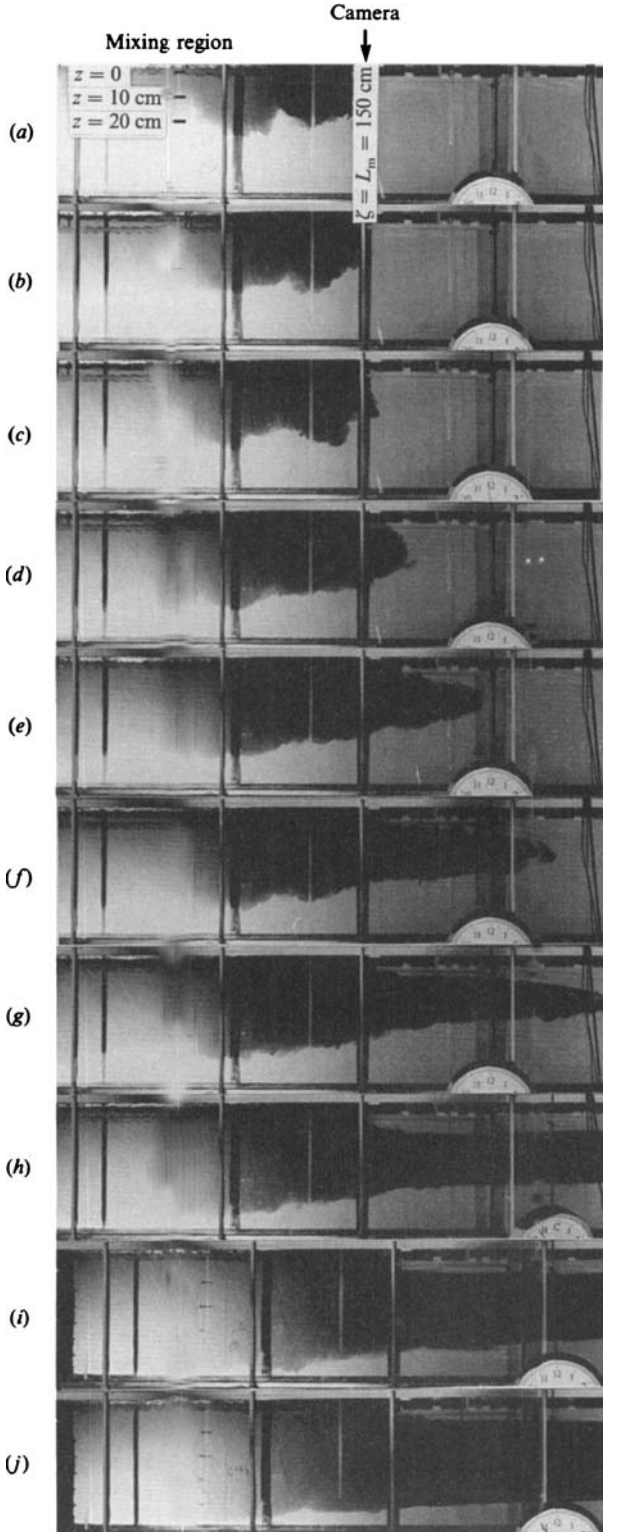

FIGURE 7. Photographs of the mixing region for Exp 226 ($N = 0.16\ \mathrm{s}^{-1}$, $K = 81.9\ \mathrm{cm}^2\ \mathrm{s}^{-1}$, $y = 22.6$ cm) showing mixed-layer deepening and intrusion formation. These photos were taken (*a*) 9 s, (*b*) 29 s, (*c*) 39 s, (*d*) 80 s, (*e*) 132 s, (*f*) 174 s, (*g*) 205 s, (*h*) 574 s, (*i*) 847 s and (*j*) 1108 s after the grid was set in motion.

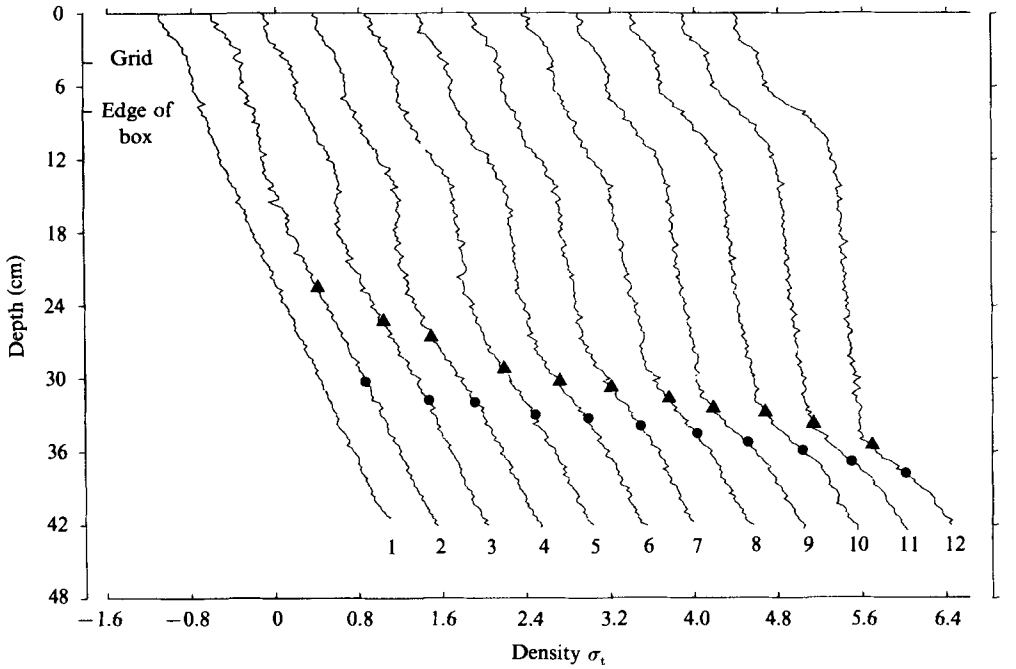

FIGURE 8. Density profiles from Exp 262 at $\zeta = 250$ cm. Times the profiles were taken are: (1) 0 s, (2) 220 s, (3) 390 s, (4) 525 s, (5) 665 s, (6) 825 s, (7) 925 s, (8) 1200 s, (9) 1600 s, (10) 2000 s, (11) 2600 s and (12) 3400 s. The approximate depths of the mixed layer in the mixing region is indicated by ●, while ▲ indicates the bottom of the outflow in the interior of the tank.

region. As can be seen from the profiles, this homogenization takes place on quite a long timescale.

An overall picture of the flow can be synthesized from the observations above, and is sketched in figure 9. Initially, the interface deepens quite rapidly (figure 9*a*). When $t \approx 2\pi N^{-1}$, collapse starts (figure 9*b*), generating internal waves. The intrusion length begins to increase as mixed fluid enters the intrusion at the edge of the mixing region. After collapse begins, the position of the interface remains constant for a short time, as long as the vertical velocity induced by the intrusion is equal to the entrainment velocity. This phase is cut short by the reflection of intrusion-generated shear waves off the far wall.

Figure 9(*c*) shows a sketch of the flow field when the first wave has reflected from the back wall but has not yet met the intrusion. A brief while later, the wave has reached the edge of the mixing region (figure 9*d*). The interface then resumes its downwards migration, albeit slowly, since the entrainment interface must now supply fluid not only to lengthen the intrusion, but also to separate isopycnals upstream of the visible head of the intrusion. Aside from the arrested progression of the intrusion head, this separation of upstream isopycnals is the most evident manifestation of rear-wall blocking. These latter processes become even more obvious when the stage shown in figure 9(*e*) is reached. Here the slug has almost reached the end of the tank; all of the entrained field is used to fatten the slug and to push down its lower interface. The fluid that enters the mixing region from below moves along isopycnal surfaces and displays the characteristics of a withdrawal layer in the classical sense (Imberger *et al.* 1976), with the mixing interface acting as a sink.

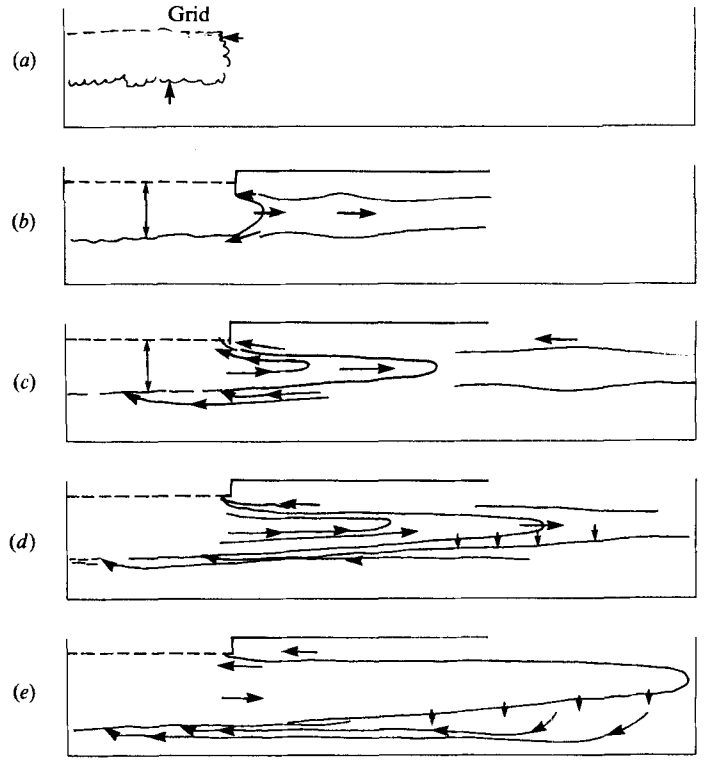

FIGURE 9. Sketches of the observed flow: (*a*) initially local mixed-layer deepening; (*b*) the development of the outflow and shear-wave generation; (*c*) the reflection of shear waves and the development of recirculation near the grid; (*d*) blocking of the outflow intrusion by reflected shear waves; (*e*) the final state of quasi-one-dimensional mixed-layer deepening.

In all our experiments, the chosen forcing method results in a strong recirculation zone close to the free edge of the grid. This flow consists of a sink withdrawing fluid from the region surrounding the grid, and from both above and within the dye-marked intrusion. This fluid is then re-injected into the intrusion. This strong reverse flow within the intrusion appeared to be independent of the position of the lower interface.

4.2. *Comparison of experimental observations with theory*

We ran 13 experiments of the type discussed above. Table 1 gives a complete tabulation of the experimental parameters. In order to cover the complete range of the observed behaviour, we have plotted two additional sets of mixed-layer depth h *vs.* t and intrusion length L *vs.* t data in figures 10 and 11. From these and similar curves, we have derived a set of parameters that characterize each experiment, which are also listed in table 1. The most useful of these derived quantities are: (i) the equilibrium depth of the interface (η_e) found that between the initial formation of the interface and the interaction of the intrusion with the return wave; and, (ii) the asymptotic (quasi-one-dimensional) rate of mixed-layer deepening as described by a curve of the form:

$$\eta^8 = a\tau + b. \tag{34}$$

For all of the experiments reported in table 1, the coefficient of correlation associated with fitting (34) to the observed data was larger than 0.98, and in some cases was as

Exp No (date)	N (s^{-1})	K ($cm^2\ s^{-1}$)	y (cm)	a observed
184	0.30	81.9	16.5	1.12
226	0.16	81.9	22.6	2.10
228	0.20	81.9	20.2	1.20
229	0.19	55.5	17.0	0.44
230	0.28	63.0	15.0	0.32
234	0.23	63.0	16.6	0.33
235	0.10	46.5	21.6	2.00
241	0.38	46.5	11.0	0.91
244	0.38	63.0	13.0	0.32
257	0.30	46.5	12.4	1.73
262	0.23	50.0	14.7	1.11
270	0.38	47.1	11.1	0.98
277	0.44	47.1	10.2	0.59

TABLE 1. Experimental data and results: linear stratifications

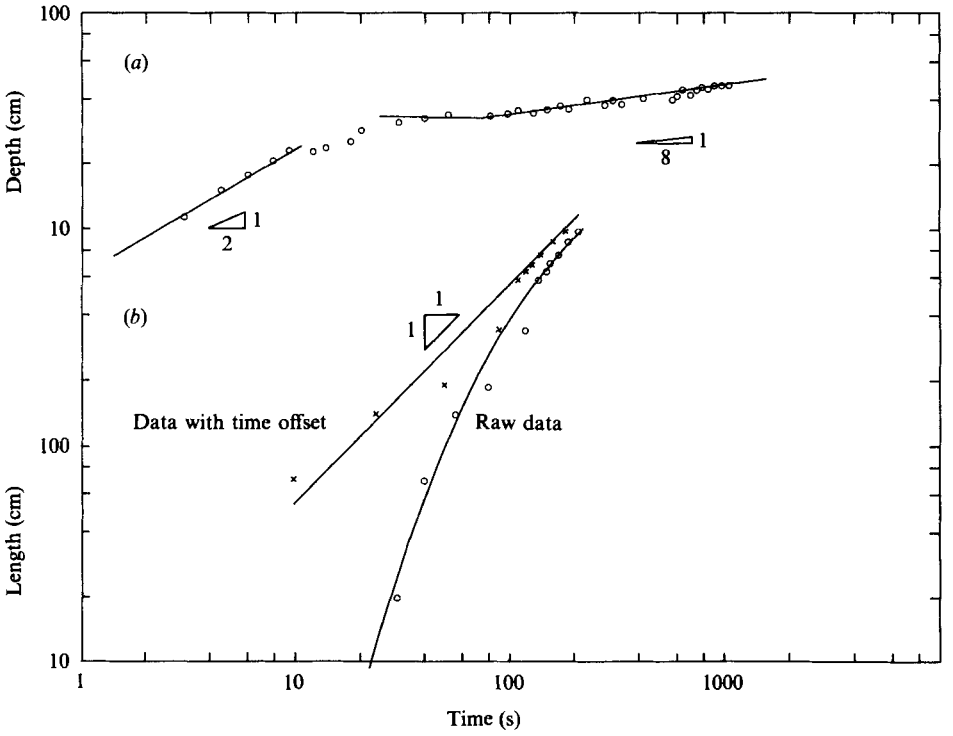

FIGURE 10. (*a*) Mixed-layer depth and (*b*) intrusion length as functions of time for Exp 226.

high as 0.999 (i.e. 1), indicating that the experimental data do exhibit the time dependence predicted by (23).

The observed values of η_e are plotted in figure 12, as a function of (y/L_m). We have also drawn the line

$$\eta_e = 1.08\left(\frac{L_m}{y}\right)^{\frac{1}{6}}, \tag{35}$$

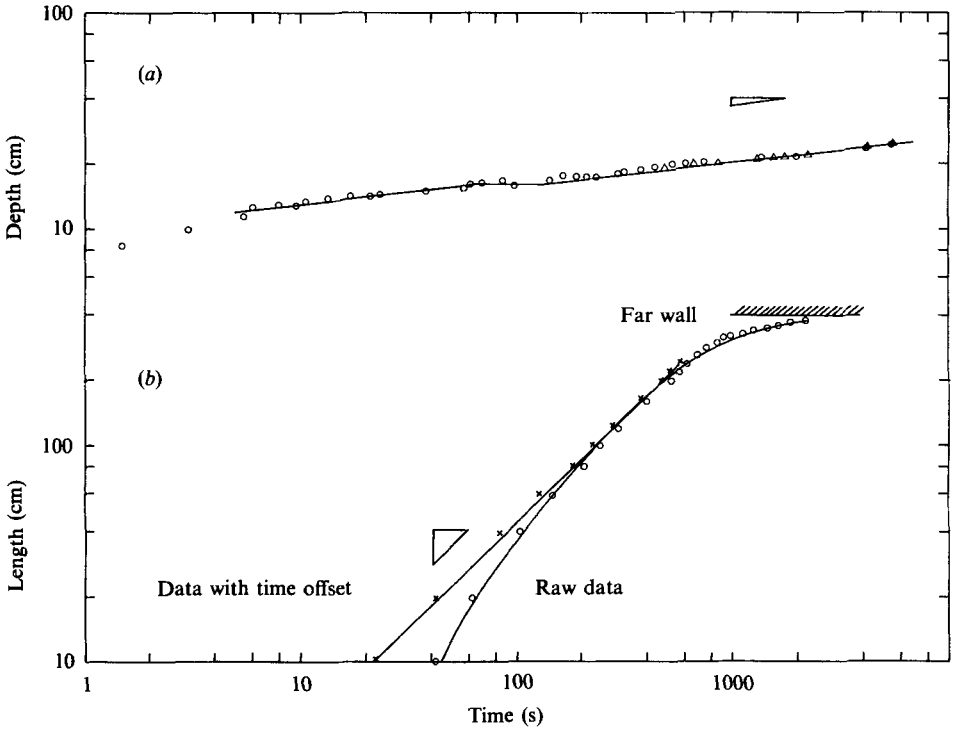

FIGURE 11. (a) Mixed-layer depth and (b) intrusion length as functions of time for Exp 277.

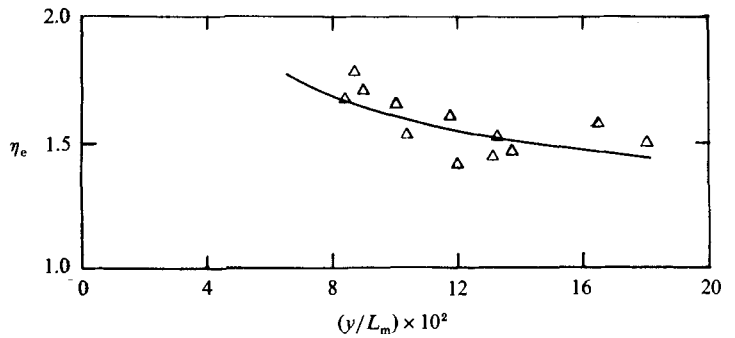

FIGURE 12. Non-dimensional equilibrium depth η_e, as a function of (y/L_m) for experiments with linear stratifications.

the relation appropriate to a viscous flow, on the plot. The fit is generally quite good, whereas it is clear that a curve of the form

$$\eta_e \sim \left(\frac{L_m}{y}\right)^{\frac{1}{9}},$$

i.e. the relation appropriate to an inertial flow, would not match the decrease in η_e with increase in (y/L_m) as well as does the viscous curve. Thus we conclude that the experiments favour the viscous–buoyancy scaling over the inertia–buoyancy scaling. Some of the scatter in the experimental points may be because the initial stratifications were never perfectly linear. In some cases, the mixed layer appeared

to stop deepening at depths near the predicted equilibrium depth, where the local density gradient was somewhat stronger than the average gradient. In other cases, regions of weaker gradient allowed the mixed layer to deepen past the equilibrium depth calculated using an average value of N.

We can express the parametrized outflow rate in terms of an 'eddy' viscosity ν_t rather than in terms of K:

$$Q'_{\text{out}} = AN^2h^5\nu_t^{-1}L_m^{-1}. \tag{36}$$

If we now set $\nu_t = 4ql_t = 0.32K$ (Hopfinger & Linden 1982), (31) allows us to determine that $A = 0.08$. This small value of A is typical of viscous–buoyancy flows such as cavity convection flows (e.g. Imberger 1974).

Results for the constant a in (34) are also in general agreement with the values predicted theoretically. The deduced values of a show no systematic variation with y; again, variations in a must be attributable to vertical variations in N. Additionally, since the fitted curve involves a calculation of y^8, any errors in measuring S and f become magnified in the calculation, because y^8 is proportional to S^6 and f^4. Using all of the experimental results, we calculate an average value of $a = 0.98$, in excellent agreement with the predicted (using $L_m/L_t = 0.23$) value of 0.95.

5. Mixing in a two-layer fluid

5.1. *Initial conditions*

Simple dimensional analysis suggests that the case of a two-layer stratification is inherently more complicated than that of a linear stratification: assuming that the virtual origin of the grid coincides with the free surface, three parameters characterize the flow when the stratification is linear: the scale length y, the length of the mixing region, and the total length of the tank. Of these only one, y, could be effectively varied in the present experiments. When the stratification is two-layered, there are instead five parameters: the scale length x, the initial mixed-layer depth, the initial interface thickness, and the two lengths mentioned above. In our two-layered experiments three of these could be varied. Because of these two extra lengthscales, our two-layered experiments showed far more variability of both deepening rates and outflow behaviour than did our experiments with linear stratifications.

5.2. *General description*

Overall, flows driven by mixing in the two-layer experiments were similar to those observed when the stratification was initially linear. Again, there was an initial phase of rapid, localized deepening, followed by a second phase of equilibration and outflow, and a final phase of nearly uniform deepening.

The principal difference between the two types of experiments is the structure of the shear-wave modes, which depends on the density profile. The most striking manifestation of this difference was the generation of second-mode solitary waves, i.e. interfacial bulges (see Maxworthy 1980), by the outflow intrusion in the two-layered experiments. In several experiments (284, 287, 302 and 305) these waves separated from the intrusion, were reflected off the back wall, and travelled back towards the mixing region. When these waves made contact with the front of the intrusion, the intrusion stopped moving. In one case (302) the nose of the intrusion was split in two by the reflected waves! Figure 13(*a*, *b*) shows such a wave approaching the mixing region from the left. In figure 13(*a*) the crest of the wave, which appears as a bulge in the outflow intrusion, is located at the far right of the

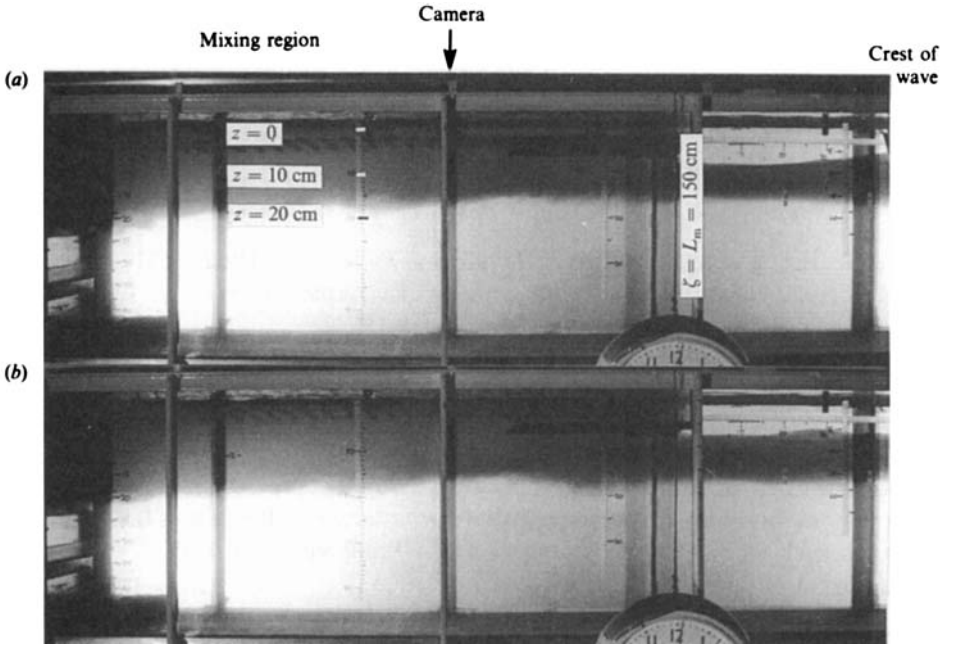

FIGURE 13. Reflected shear waves approaching the mixing region for Exp 302.

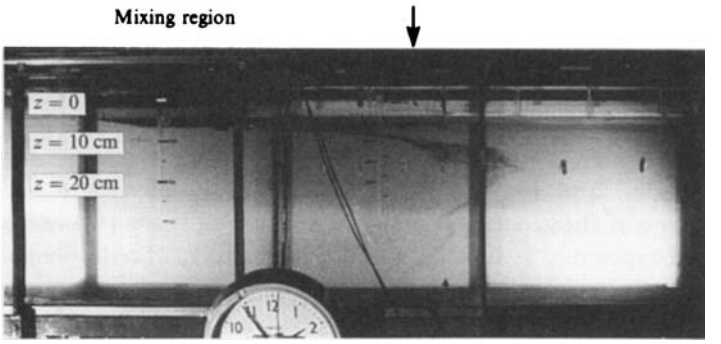

FIGURE 14. The quasi-steady velocity profile at the edge of the mixing region for Exp 304.

photo. In figure 13(*b*), taken approximately 20 s after figure 13(*a*), the crest of the wave is at $x = 30$ cm, although the wave is losing its shape. Note that the thickness of the outflow region increases by about 3 cm between figure 13(*a*) and 13(*b*) when the wave arrives. These are large-amplitude forms of the shear waves seen in the linear experiments, playing exactly the same role: they signal the presence of the far wall to the mixing region.

The steady-state velocity profile in figure 14 shows two circulation cells. The upper cell consists of inflow into the upper part of the mixed region and some of the outflow from the lower part of the mixed region. The lower cell is made up of outflow from the mixed region and some stress-driven flow in the interface and the lower layer; these are balanced by a sink flow towards the mixing region in the lower part of the lower layer. In contrast, in the linearly stratified experiments the recirculating entrainment flow was confined to a narrow layer below the entrainment interface.

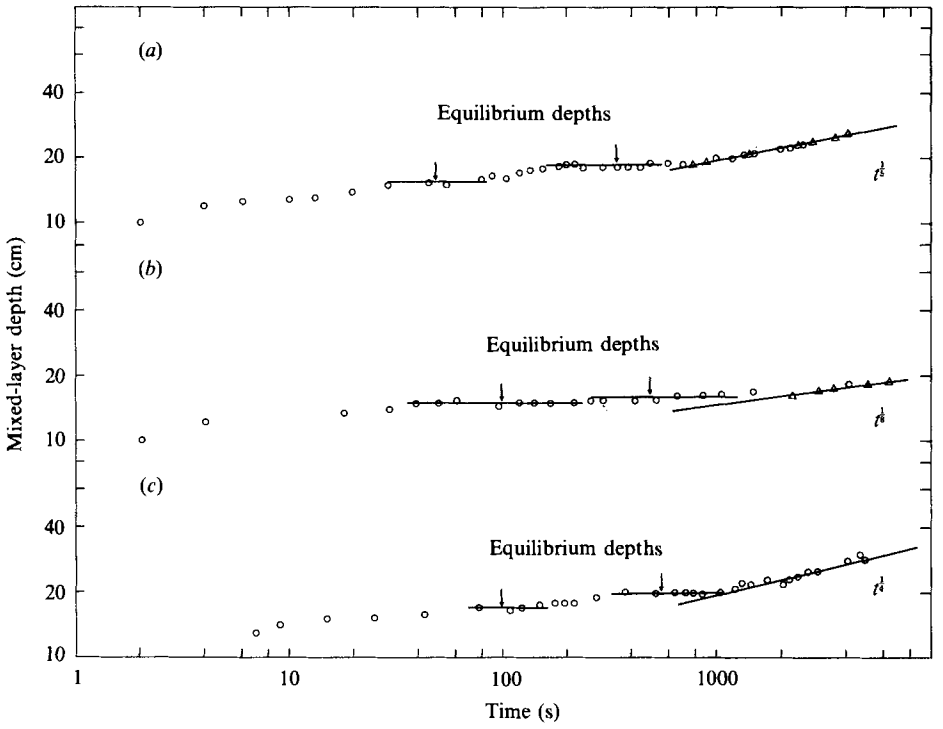

FIGURE 15. Mixed-layer depth as a function of time for (*a*) Exp 302, (*b*) Exp 304 and (*c*) Exp 305.

Figure 15 shows samples of mixed-layer depths plotted as functions of time for three experiments with two-layered stratifications. Again, deepening takes place in three phases: initial rapid deepening, equilibration and asymptotic, quasi-one-dimensional deepening.

As in experiments with linear stratifications, the equilibration process did not quite unfold as assumed in theory: several equilibrium depths were observed and the mixed-layer depth varied somewhat across the mixing region. For example, in Exp 302, the mixed layer first stops deepening for approximately 30 s when $h = 15.5$ cm ($\eta = 1.8$), and then resumes deepening until it reaches a new equilibrium at $h = 18$ cm ($\eta = 2.1$); this depth is maintained for a further 200 s, until the outflow intrusion has become blocked by the rear wall. The occurrence of multiple equilibrium depths is probably due to partial blocking of the outflow, i.e. the interaction of the intrusion with the first (fastest) shear waves to be reflected off the far wall.

Several of the plots of outflow length as functions of time shown in figure 16 do not exhibit any of the simple power-law dependencies measured in intrusion experiments (e.g. Maxworthy 1972, 1983). Curves for Exps 303 and 304 both show the intrusion slowing down and then speeding up. As before, this behaviour can be attributed to the interaction of the intrusion with reflected shear waves.

Figure 17 shows the evolution of the density field as exemplified by profiles measured at two stations during Exp 306. These profiles show how a mixed layer forms and initially deepens under the grid (profile 2) while the interior of the tank remains unaffected. Next, even before the intrusion arrives at the interior measuring station (profile 3), the interface thickens, presumably because of rear-wall blocking

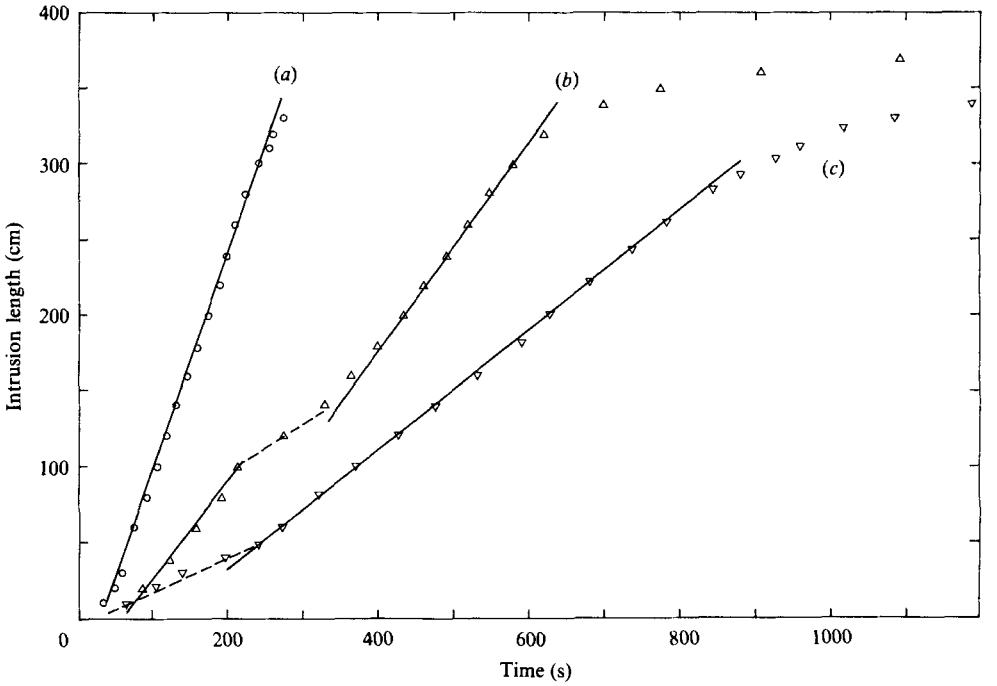

FIGURE 16. Intrusion length as a function of time for (*a*) Exp 302, (*b*) Exp 303 and (*c*) Exp 304.

of the intrusion. Once the intrusion has reached the measuring station, the interface thickens with a concomitant weakening of the interfacial density gradient. Contrary to the homogeneity assumed in calculating the outflow rate in §3, the outflow is still stratified at this point. In the final deepening phase, the interface continues to thicken and to homogenize. The upper interface seen in figure 17 is an unavoidable consequence of the experimental geometry.

An examination of the density profiles measured in the mixing region shows that the interface thickness was quite variable; this is consistent with many observations of the entrainment process (see Crapper & Linden 1974 or Fernando & Long 1985) that show the interface as alternately sharpened (scoured) and diffused by mixing events. However, as seen in those profiles taken outside the mixing region, the interface, which corresponds to the edge of the dyed region, is virtually non-existent in the sense that no step can be seen. This implies that an important difference exists between true one-dimensional deepening by stirring and the quasi-one-dimensional deepening process we observe: the quasi-one-dimensional deepening process does not result in interfacial sharpening.

5.3. *Comparison of experiment and theory*

Table 2 presents a summary of the experimental conditions for the two-layered experiments. For each experiment, the interface thickness was derived from the initial profile by determining the elevations at which a line colinear with the slope of the density profile in the middle of the interface intersects the vertical lines colinear with the density profile in the upper and lower layers.

Because we have not presented any theory for the equilibration process in a two-layered fluid, the experimental results for two-layer stratifications are summarized

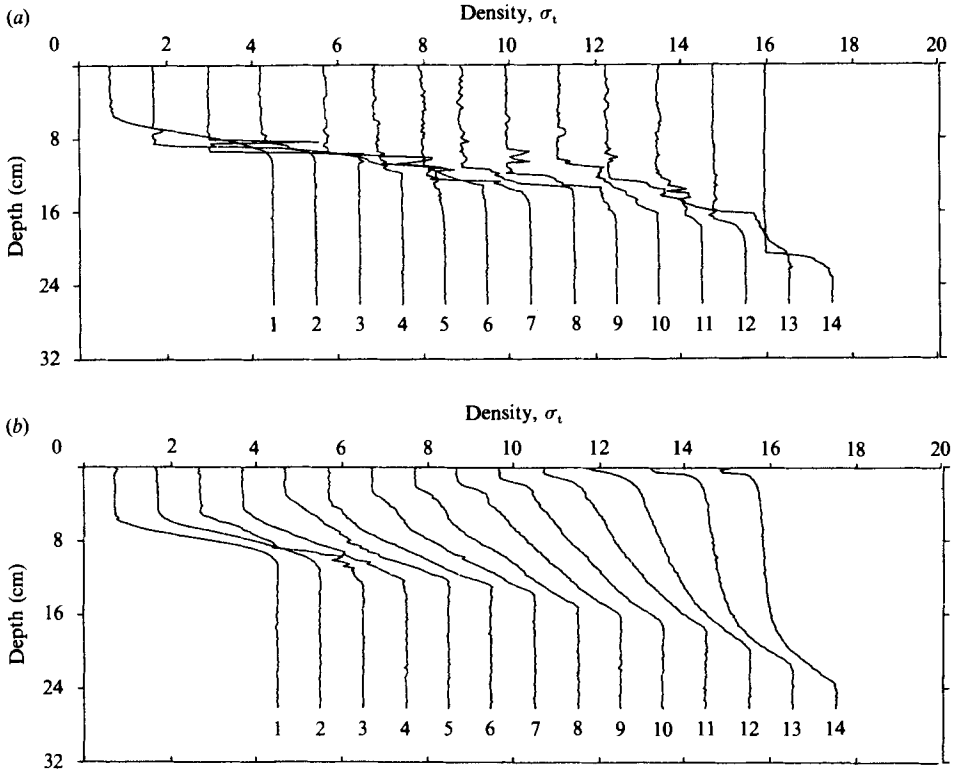

FIGURE 17. Density profiles in Exp 306 at (*a*) $\zeta = 105$ cm, and (*b*) $\zeta = 285$ cm. The profiles were taken at the following times: (1) 0 s, (2) 15 s, (3) 55 s, (4) 110 s, (5) 210 s, (6) 270 s, (7) 340 s, (8) 390 s, (9) 905 s, (10) 640 s, (11) 905 s, (12) 1213 s, (13) 1490 s, (14) 1880 s, (15) 3740 s and (16) 5720 s. Each profile is offset by $1.0\sigma_t$.

Exp No. (date)	g' cm s^{-2}	h_0 cm	K cm^2 s^{-1}	δ_i cm	x cm	a predicted	a observed	k observed
284	7.3	5.0	46.5	3.1	7.5	0.92	1.85	0.20
287	6.2	10.0	47.4	4.3	5.8	0.024	0.020	0.20
302	6.2	9.5	67.1	1.5	8.6	0.096	0.042	0.20
303	3.3	9.0	38.5	2.0	6.9	0.074	0.043	0.20
304	7.3	12.0	38.2	4.0	4.3	—	—	0.13
305	2.3	11.7	66.8	2.4	13.6	—	—	0.23
306	4.5	11.7	67.1	3.1	9.8	—	—	0.14

TABLE 2. Experimental data and results: two-layer experiments

δ_i = initial interface thickness; k = observed exponent in asymptotic one-dimensional deepening law i.e. $h \sim t^k$.

only in terms of (i) the exponent k in the asymptotic deepening law $h \sim t^k$; and, (ii) when $k = 0.2$, the constant of proportionality (by analogy with (34)).

Figure 15 illustrates the range of values found for the exponent k in the asymptotic deepening law (i.e. $h \sim t^k$). The predicted form of this law, $k = 0.2$, is only seen in Exp 302; $k = 0.13$ in Exp 304; and $k = 0.25$ in Exp 305. These variations in k have two sources: first, the theory assumes that $x < h$ ($\eta > 1$); second, the theory assumes

that the interface has zero thickness. In Exp 304, although x was less than the initial mixed-layer depth, it was only marginally larger than the interface thickness. Thus, the mixed layer was actually deepening into a linear stratification. This conclusion is supported by the fact that the observed deepening is consistent with that expected of a linearly stratified fluid.

In Exp 305, x was larger than the initial mixed-layer depth; hence, $Ri = (h/x)^2$ was small enough for the deepening rate to approach that expected of an homogeneous fluid. In terms of the turbulent-kinetic-energy budget expressed by (1), the 'spin-up' of fluid (Denton & Wood 1982), represented by the constant in the denominator of (1), required an amount of turbulent kinetic energy comparable with that expended by working against gravity to entrain heavier fluid (the $Ri^{\frac{3}{2}}$ term).

Table 2 lists the predicted and observed asymptotic deepening rates only for those experiments in which $k = 0.2$. The agreement between theory and observations is not nearly as good as that for experiments with linear stratifications. While there is less agreement between the individual predicted and observed values of a (where for two-layer stratifications, $\eta^5 = a\tau + b$), the average ratio of predicted to observed deepening rates is quite close to 1 (0.97), indicating a reasonable agreement between theory and observation. From the observations summarized in table 2, we can conclude that the theory presented in §2.3 is most accurate when the interface is thin and when the scale depth x is not larger than the initial mixed-layer depth.

6. Discussion

In this section, we shall apply the results of our study (most notably (36)) to examine the effects of spatially variable mixing on mixed-layer deepening for the two 'real-life' flows described in §1. The purpose of this exercise is to see whether or not mixed-layer equilibration, as we observe it in the laboratory, is likely to occur in nature.

To apply our results to natural mixing processes, it is necessary to specify appropriate entrainment laws. As discussed in Sherman *et al.* (1978), and Imberger (1985), when boundary-generated turbulence (stirring) drives mixed-layer deepening,

$$u_e = C_1 u_* Ri^{-1}, \tag{37}$$

whereas when deepening is driven by interfacial shear,

$$u_e = C_2 u_* Ri^{-\frac{1}{2}}, \tag{38}$$

where $Ri = g'h_0/u_*^2$. The constants C_1 and C_2 are approximately 0.1 (e.g. Kranenburg 1985) and 0.3 (Spigel, Imberger & Rayner 1986). We may assume that $\nu_t = 0.1hu_*$ (Fischer *et al.* 1979). Thus, for linearly stratified fluids,

$$h_e = \left(\frac{0.2C_1}{A}\right)^{\frac{1}{6}} \left(\frac{u_*}{N}\right)^{\frac{2}{3}} L_m^{\frac{1}{3}} = 0.8X^{\frac{2}{3}} L_m^{\frac{1}{3}}, \tag{39}$$

in the first case; the scale depth X is defined by the relation

$$X = \frac{u_*}{N}. \tag{40}$$

In the second case,

$$h_e = 1.0X^{\frac{3}{5}} L_m^{\frac{2}{5}}. \tag{41}$$

For tidal flows with negligible shear, $u_* = C_D^{\frac{1}{2}} U$, so that (39) becomes

$$\frac{h_e}{H} = C_D^{\frac{1}{3}} \left(\frac{U}{NH}\right)^{\frac{2}{3}} \left(\frac{L_m}{H}\right)^{\frac{1}{3}}. \tag{42}$$

Thus, $(h_e/H) = 1$, i.e. a front will form when $U/NH \sim (C_D L_m/H)^{-\frac{1}{2}}$, rather than when $U/NH =$ a constant, as derived by Maxworthy (1984), unless $L_m \sim H$. Here L_m must be the scale over which U varies significantly. Simpson *et al.* (1982) present observations of mixing produced by a submerged island; in that case, the mixing is very nearly discontinuous, as in the present set of experiments. Assuming $C_D = 10^{-2}$, $L_m = 100$ km, $H = 100$ m, we find $(h_e/H) = 1$ (for $u_* =$ a constant) when $U/NH = 0.6$, a value somewhat smaller than that (2.0) derived by Maxworthy (1984) in analysing the Simpson & Hunter (1974) data. This suggests that unsteadiness in the mixing rate due to tidal variations in u_* is important because the time required to reach equilibrium is longer than the duration of mixing. We can write an expression for $\mathrm{d}h/\mathrm{d}t$, including the effects of outflow, in terms of $\eta = h/H$, and $\tau = Nt$; viz:

$$\frac{\mathrm{d}\eta}{\mathrm{d}\tau} = 0.2\left(\frac{X}{H}\right)^3 \eta^{-2} - 0.8(H^3 X^{-1} L_m^{-2})\,\eta^4. \tag{43}$$

Integration of (43) shows that the actual time taken to reach equilibrium is infinite. However, the time τ_δ required to reach any particular value of $(\eta/\eta_e) = \delta$ is

$$\tau_\delta = 0.4\left(\frac{L_m}{X}\right) \ln\{(1+\delta^3)(1-\delta^3)^{-1}\}. \tag{44}$$

For example, for $\delta = 0.99, \tau_\delta = 1.7(L_m/X)$. Using numbers appropriate to a tidal front, we find that this corresponds to a time of 16 days, which is significantly longer than the tidal period. Thus, the equilibrium depth is also a function of the tidal period (non-dimensionalized by N) as well as the r.m.s. tidal velocity.

The case of differential mixed-layer deepening in lakes is more difficult to analyse than that of tidal mixing because of the complex structure of wind-sheltering patterns which give rise to differential mixing (Imberger & Parker 1985). To proceed, it is first necessary to know which entrainment law, (37) or (38), is appropriate. According to Spigel & Imberger (1980), this choice of entrainment laws depends on the value of the Wedderburn number,

$$W = Ri\frac{h}{L},$$

where Ri is defined as above and L is the length of the basin in the direction of the wind. If $W > 1$, (37) is valid, whereas if $W < 1$, (38) is valid.

For an initially linear stratification, $W = 0$ (Monismith 1986), and the second relation is valid. However, as the layer deepens, W increases, so that when

$$h > 2X^2 L = h_{\mathrm{shear}},$$

the mixing process switches over from one dominated by shear to one dominated by stirring (assuming that equilibration takes place before the shear is cut off by pressure effects – see Spigel *et al.* 1986). Because of this, the mixed-layer response may change with time, even with a constant wind stress. The equilibrium depth will be given by (41) if the predicted value of h_e is less than h_{shear}. On the other hand, if the predicted value of h_e is greater than h_{shear}, the mixed layer would first deepen to $h = h_{\mathrm{shear}}$, whence the deepening rate would start to decrease while the outflow rate

remained constant. The mixed-layer depth would then decrease towards the value given by (40) (which is generally less than that given by (41)). However, if h drops below h_{shear}, the mixing rate would increase; equilibration would therefore appear to take place at a depth near h_{shear}.

To put this in perspective, we consider typical values of the relevant parameters for the case of a surface layer of a reservoir (e.g. Imberger & Parker 1985). We set $u_* = 5 \times 10^{-3}$ ms^{-1}, $N = 3 \times 10^{-2}$ s^{-1} and $L_{\text{m}} = L = 1$ km, giving $h_{\text{e}} = 5.4$ m if (41) is valid, $h_{\text{e}} = 2.4$ m if (40) is valid, and $h_{\text{shear}} = 4.7$ m. Thus, according to the arguments given in the preceding paragraph, we would predict equilibration at $h \sim 5$ m. Again, since the wind may not blow long enough for the mixed layer to reach its equilibrium, and because shear-driven deepening only persists for a time less than $\frac{1}{4}$ of the appropriate internal seiche period (Imberger 1985), this estimate must be to some degree an overprediction. Indeed, the observations presented in Imberger & Parker (1985) show horizontal variations in mixed-layer depth of 2 to 3 m rather than 5 m as suggested above.

It should be pointed out that the experimental and theoretical results are sensitive to the spatial decay of grid turbulence. Furthermore, two potentially important effects have been ignored in the present study: the effect of rotation on the observed flows, and, as pointed out above, the likely effects of temporal non-uniformity of the mixing process.

Rotation is likely to be crucial in determining the motion of the outflow from the mixed region, since both the inflow and outflow are set up by waves characterized by small Rossby radii, $L_{\text{R}} = C/f$, where C is the wave speed and f is the Coriolis parameter. For the flows discussed above, L_{R} typically will be between 100 and 1000 m. Where the outflow takes place next to a solid boundary, intense 'Kelvin' currents (currents in which the cross-stream Coriolis force is balanced by a cross-stream pressure gradient supported by the wall) can be formed. In the case of tidal mixing, L_{R} must set the offshore width of the outflow and inflow. Evidence for this behaviour comes from intrusion experiments reported by Maxworthy (1982) and from boundary-mixing experiments described by Ivey (1987). For the case of an enclosed basin, such as a reservoir, the spatial structure of the inflow–outflow currents would be quite complex, as demonstrated by the withdrawal experiments discussed in Monismith & Maxworthy (1987). Based on Griffiths & Linden's (1982) and Ivey's (1987) experiments, it should be expected that the outflow intrusion would become rotationally unstable, leading to the formation of large vortices with concomitant offshore transport of mixed fluid. It is unclear whether rotation influences the amount of fluid leaving the mixing region since scaling arguments similar to those given in §2 show that Coriolis forces are of the same magnitude as frictional forces.

In the case of tidal mixing, the tidal variation of the flow velocity appears to be an important factor in determining the location of the front. As the current accelerates, the mixed layer deepens; if it fails to surface (or reach its equilibrium depth) before the current starts to decelerate, it tends to become shallower, i.e. retreat, as soon as the outflow exceeds the entrainment flow. Temporal non-uniformities in the intensity of mixing should also result in the formation of quite complex outflow structures due to the interaction of shear waves generated by changes in outflow, with the outflow itself. The lake example presented also suggests that unsteadiness of the mixing rate is important. Clearly, the unsteady case warrants further study.

7. Conclusions

Both experimentation and theory make clear that differential deepening takes place in three phases: an initial phase of one-dimensional deepening; an equilibrium phase wherein the mixed-layer depth remains constant until the outflow from the mixed layer is blocked by the back wall; and a final phase in which the mixed layer no longer deepens differentially, but instead deepens at a rate that is the product of the one-dimensional entrainment velocity in the mixing region and the fraction of the total length over which active mixing is taking place. Excepting the initial collapse process that produces the outflow, the outflow rate appears to be set by a balance of turbulent shear stresses and the pressure gradient associated with the density gradient created by differential mixing. Finally, the general effects of differential mixing, as just outlined, are found when the fluid is stratified either linearly or as two homogeneous layers.

This work was jointly sponsored by the Centres for Water Research and Environmental Fluid Mechanics at the University of Western Australia; it was performed while the first author (T.M.) was visiting the University of Western Australia as a Senior Queen's Fellow in the Marine Sciences. We thank the technical staffs of the two Centres and of the Dept. of Civil Engineering at the University of Western Australia for their help. We are grateful to L. Armi, A. Dittrich, L. Freeman, J. Taylor, and the reviewers for their comments concerning this paper. We also wish to thank Professor Jörg Imberger for his support and efforts in making this study possible.

REFERENCES

AMEN, R. & MAXWORTHY, T. 1980 The gravitational collapse of a mixed region into a linearly stratified fluid. *J. Fluid Mech.* **96**, 65–92.

ARMI, L. 1986 The hydraulics of two flowing layers with different densities. *J. Fluid Mech.* **163**, 27–58.

BATCHELOR, G. K. 1967 *An Introduction to Fluid Dynamics.* Cambridge University Press.

CRAPPER, P. F. & LINDEN, P. F. 1974 The structure of turbulent density interfaces. *J. Fluid Mech.* **65**, 45–64.

DENTON, R. A. & WOOD, I. 1982 Penetrative convection at low Péclet number. *J. Fluid Mech.* **113**, 1–21.

FERNANDO, H. J. S. & LONG, R. R. 1985 On the nature of the entrainment interface of a two-layer fluid subjected to zero-mean-shear turbulence. *J. Fluid Mech.* **151**, 21–53.

FISCHER, H. B., LIST, E. J., KOH, R. C. Y., IMBERGER, J. & BROOKS, N. H. 1979 *Mixing in Inland and Coastal Waters.* Academic.

FOSTER, M. E. & SAFFMAN, P. G. 1970 The drag of a body moving transversely through a confined stratified fluid. *J. Fluid Mech.* **43**, 407–418.

GRIFFITHS, R. W. & LINDEN, P. F. 1982 The stability of vortices in a rotating stratified fluid. *J. Fluid Mech.* **105**, 283–316.

HOPFINGER, E. J. & LINDEN, P. F. 1982 Formation of thermoclines in zero-mean-shear turbulence. *J. Fluid Mech.* **114**, 157–173.

HOPFINGER, E. J. & TOLY, J. A. 1976 Spatially decaying turbulence and its relation to mixing across density interfaces. *J. Fluid Mech.* **78**, 155–175.

IMBERGER, J. 1974 Natural convection in a shallow cavity with differentially heated end wall. Part 3. Experimental results. *J. Fluid Mech.* **65**, 247–260.

IMBERGER, J. 1982 Reservoir dynamics modelling. In *Predictions in Water Quality* (ed. E. M. O'Loughlin & P. Cullen). Canberra: Australian Academy of Science.

IMBERGER, J. 1985 The diurnal mixed layer. *Limnol. Oceanogr.* **30**, 737–770.

IMBERGER, J. & PARKER, G. 1985 Mixed layer dynamics in a lake exposed to a spatially variable wind field. *Limnol. Oceanogr.* **30**, 473–489.

IMBERGER, J., THOMPSON, R. O. R. Y. & FANDRY, C. 1976 Selective withdrawal from a finite rectangular tank. *J. Fluid Mech.* **78**, 489–512.

IVEY, G. N. 1987 Boundary mixing in a rotating stratified fluid. *J. Fluid Mech.* **183**, 25–44.

IVEY, G. N. & CORCOS, G. M. 1982 Boundary mixing in a stratified fluid. *J. Fluid Mech.* **121**, 1–26.

KRANENBURG, C. 1979 Destratification of lakes using bubble columns. *J. Hydraul. Div. ASCE* **105** (HY4), 333–349.

KRANENBURG, C. 1985 Mixed-layer deepening in lakes after wind set-up. *J. Hydraul. Div. ASCE* **111** (HY9), 1279–1297.

LINDEN, P. F. 1975 The deepening of a mixed layer in a stratified fluid. *J. Fluid Mech.* **71**, 385–405.

LONG, R. R. 1978 A theory of mixing in stably stratified fluids. *J. Fluid Mech.* **84**, 113–124.

MANINS, P. C. 1976 Intrusion into a statified fluid. *J. Fluid Mech.* **74**, 547–560.

MAXWORTHY, T. 1972 Experimental and theoretical studies of horizontal jets in a stratified fluid. *Intl Symp. of Stratified Fluids*, Novosibirsk, USSR.

MAXWORTHY, T. 1980 On the formation of nonlinear internal waves from the gravitational collapse of mixed regions in two and three dimensions. *J. Fluid Mech.* **96**, 47–64.

MAXWORTHY, T. 1982 Experiments on solitary internal Kelvin waves. *J. Fluid Mech.* **129**, 365–383.

MAXWORTHY, T. 1983 Gravity currents with variable inflow. *J. Fluid Mech.* **128**, 247–257.

MAXWORTHY, T. 1984 On the formation of tidal mixing fronts. *Ocean Modelling* **55**, 8–10.

MONISMITH, S. G. 1986 An experimental study of the upwelling response of stratified reservoirs to surface shear stress. *J. Fluid Mech.* **171**, 407–439.

MONISMITH, S. G. & MAXWORTHY, T. 1987 The effect of rotation on selective withdrawal from a point sink. *Preprints for the Third Intl Symp. on Stratified Flows, Pasadena, Feb. 3–5, 1987*, vol. 3.

SHERMAN, F. S., IMBERGER, J. & CORCOS, G. M. 1978 Turbulence and mixing in a stably stratified waters. *Ann. Rev. Fluid Mech.* **10**, 267–288.

SIMPSON, J. E. 1982 Gravity currents in the laboratory, atmosphere, and ocean. *Ann. Rev. Fluid Mech.* **14**, 213–234.

SIMPSON, J. H. & HUNTER, J. R. 1974 Tidal fronts in the Irish Sea. *Nature* **250**, 404–406.

SIMPSON, J. H., TETT, P. B., ARGOLE-ESPINOZA, M. L., EDWARDS, A., JONES, K. J. & SAVIDGE, G. 1982 Mixing and phytoplankton growth around an island in a stratified sea. *Continental Shelf Res.* **1**, 15–32.

SPIGEL, R. H. & IMBERGER, J. 1980 The classification of the mixed-layer dynamics in lakes of small to medium size. *J. Phys. Oceanogr.* **10**, 1104–1121.

SPIGEL, R. H., IMBERGER, J. & RAYNER, K. N. 1986 Modelling the diurnal mixed layer. *Limnol. Oceanogr.* **31**, 533–556.

STILLINGER, D. C., HELLAND, K. N. & VAN ATTA, C, W. 1983 Experiments on the transition of homogeneous turbulence to internal waves in a stratified fluid. *J. Fluid Mech.* **131**, 91–122.

TURNER, J. S. 1968 The influence of molecular diffusivity on turbulence and entrainment across a density interface. *J. Fluid Mech.* **33**, 639–656.

TURNER, J. S. 1973 *Buoyancy Effects in Fluids.* Cambridge University Press.

WU, J. 1969 Mixed region collapse with internal wave generation in a density stratified medium. *J. Fluid Mech.* **35**, 531–544.